A Molecular Diode with a Statistically Robust Rectification Ratio of Three Orders of Magnitude

Li Yuan,[†] Rochus Breuer,[‡] Li Jiang,[†] Michael Schmittel,[‡] and Christian A. Nijhuis*[,†,§]

[†]Department of Chemistry, National University of Singapore, 3 Science Drive 3, Singapore 117543

[‡]Department of Chemistry and Biology, Universität Siegen, Siegen, Germany D-57068

[§]Graphene Research Centre, Centre for Advanced 2D Materials and Graphene Research Centre, National University of Singapore, 6 Science Drive 2, Singapore 117546

Ⓢ Supporting Information

ABSTRACT: This paper describes a molecular diode with high, statistically robust, rectification ratios R of 1.1×10^3. These diodes operate with a new mechanism of charge transport based on sequential tunneling involving both the HOMO and HOMO−1 positioned asymmetrically inside the junction. In addition, the diodes are stable and withstand voltage cycling for 1500 times, and the yield in working junctions is 90%.
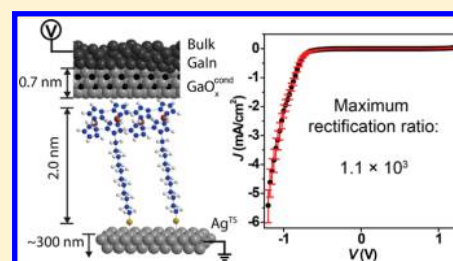
KEYWORDS: Molecular diode, tunnelling junctions, rectification ratio, molecular orbitals

Molecular electronics is complementary to conventional Si-based electronics and may induce electronic function, for example, quantum interference,[1,2] quantum plasmonics,[3,4] or giant magnetoresistance,[5] which is otherwise difficult to obtain with conventional Si-based technology.[6−13] On the other hand, relatively straightforward operations, such as the rectification of currents, are remarkably difficult to perform with molecular electronic junctions. Indeed, most molecular diodes based on, for instance, asymmetric molecule−electrode contacts,[14−16] embedded dipoles (or push−pull molecules),[17] donor−bridge−acceptor moieties (following the original design by Ratner and Aviram[18]), or one asymmetrically positioned donor or acceptor group inside the junction,[19−21] yielded so far rectification ratios $R = |J(V_{\text{for}})/J(V_{\text{rev}})| < 10$ (V_{for} = forward bias; V_{rev} = reverse bias; J = current density in A/cm^2).[22−25] Stadler et al.[23] showed theoretically that molecular diodes in the coherent tunneling regime likely cannot achieve values of $R > 20$.

A few exceptions exist, though. For instance Metzger et al.[24] reported high R values of 2−30 in junctions consisting of well-characterized Langmuir−Blodgett monolayers of electron donor−bridge−acceptor moieties with evaporated Au top-contacts. Venkataraman et al.[26] reported large values of R in single molecule junctions of up to 200 in STM break junctions. Ashwell et al.[27] used STM-tips to contact complex molecular architectures assembled into ill-defined layers of donor and acceptor molecules with very high values of R of 3000 for one junction. The lack of statistical confidence in Ashwell's data makes it impossible to determine the reproducibility, the statistical significance of the value of R, or the mechanism of charge transport. We have studied molecular diodes consisting of SAMs of SC$_{11}$Fc (Fc = ferrocenyl) supported by ultraflat

template-stripped (TS) Ag bottom electrodes in noncovalent contact (denoted by "//") with GaO$_x^{\text{cond}}$/EGaIn top-electrodes earlier.[28−31] These diodes (based on one asymmetrically positioned donor group, the Fc moiety, inside the junction) have been well characterized and they rectify currents with a value of R of about 100, while those junctions with SAMs lacking the Fc headgroup, that is, 1-undecanethiolate (SC$_{10}$CH$_3$), do not rectify.[31] For these diodes to work optimally, that is, high values of R, it is important to optimize both the electronic (especially the coupling of the Fc units to the electrodes)[28] and the supramolecular structure of the junctions (for example, the roughness of the electrode materials,[28] purity of the SAM precursor,[32] and the SAM packing[29]). Thus, it is important to optimize every aspect of the junctions to maximize the values of R.

Although molecular diodes based on a single donor moiety work well, molecular diodes based on two energetically accessible molecular energy levels are promising to yield high values of R. Molecular diodes with both donor (where the highest occupied molecular orbital (HOMO) is localized) and acceptor (where the lowest unoccupied molecular orbital (LUMO) is localized) moieties (symmetrically or asymmetrically positioned inside the junctions) have been studied before,[18,21,23−25,27,33] but controlling the energy level alignment of both the HOMO and LUMO with respect to each other and to the Fermi-levels of both electrodes is challenging.[11,23,34] The question whether the two energy levels that participate in the mechanism of charge transport have to be a LUMO and
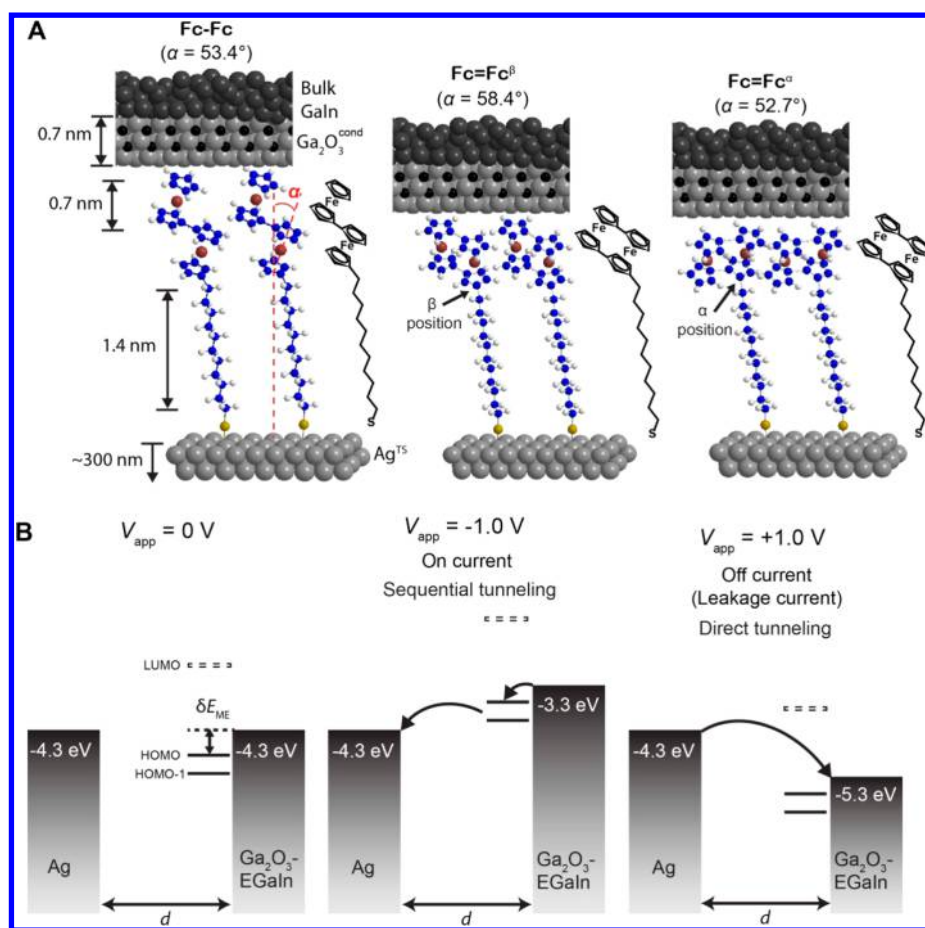
Figure 1. (A) Schematic illustrations of the junctions of Ag^{TS}-$SC_{11}Fc_2$//$Ga_2O_3^{cond}$/EGaIn. The $Ga_2O_3^{cond}$ is a 0.7 nm thick self-limiting oxide layer primarily consisting of $Ga_2O_3^{cond}$ with a very low resistance ($\sim 10^{-4}$ $\Omega\cdot cm^2$),[51−53] the SAM//$Ga_2O_3^{cond}$ contact resistance is negligible,[52] and the $Ga_2O_3^{cond}$ layer is too thin to support depletion layers.[45,54] The chemical structure of each molecule is shown at the right side of the junctions. The tilt angle of the Fc unit (α) with respect to the surface normal is defined with red dashed line. (B) The energy level diagrams at 0, − 1.0, and +1.0 V bias. The black bar indicates the HOMO and HOMO−1 positions. The dashed bar indicates the LUMO position and the dotted line indicates the Fermi-level. The arrows indicate the bias dependent change in the mechanism of charge transport.

HOMO or whether a diode based on two energetically closely spaced filled (HOMO and HOMO−1) or empty (LUMO and LUMO+1) orbitals can improve the values of R has not been experimentally addressed. However, the control of the energy level alignment of such diodes may be less cumbersome than diodes based on donor−acceptor moieties.

Here we report on the bias dependency of three types of molecular diodes with values of R as high as 1.1×10^3 based on two closely spaced molecular orbitals (the HOMO and HOMO−1) asymmetrically positioned inside the junctions. We derive our conclusions from large data sets of 450−524 $J(V)$ curves obtained from 20 junctions (Table S1), which were fabricated with a yield of ~90% in nonshorting junctions for each type of junction. These diodes consist of SAMs made from various $HSC_{11}Fc_2$, with Fc_2 representing either the biferrocene (Fc−Fc) or biferrocenylene (Fc=Fc) headgroup (abbreviated as Fc−Fc, Fc=Fc^α, and Fc=Fc^β) on ultraflat template-stripped Ag bottom electrodes contacted with GaO_x^{cond}/EGaIn top-electrodes (Figure 1). The difference between Fc=Fc^α and Fc=Fc^β is that the alkyl chain is connected to either the α or β position of the Fc, which has a large effect on the packing structure of the SAMs and the tilt angle α. We achieved these high values of R by minimizing the leakage currents (the current that flows across the junction when the diodes block the current, here at positive applied bias) via optimization of

both the supramolecular (that is, SAM packing) and electronic structure (that is, the molecule−electrode energy level alignment) of the junctions. In addition, we show that the molecular diodes are stable against voltage cycling. These diodes rectify 10 times better than diodes based on a single HOMO level asymmetrically positioned inside the junction (that is, diodes based on SAMs of $SC_{11}Fc$). We attribute this large increase in R to a mechanism of rectification involving two molecular orbitals (HOMO and HOMO−1) instead of only one (the HOMO).

The mechanism of rectification of the junctions with the $SC_{11}Fc$ SAMs have been reported before (see ref 35 for the detailed mechanism of charge transport and ref 36 for $J(V,T)$ data; this mechanism has been confirmed by others[37−39]). We believe that the mechanism of charge transport across the junctions with Fc_2 is similar as outlined in Figure 1. Figure 1 shows that the HOMO (centered at the Fc_2 unit) is in van der Waals contact with the top electrode, well separated from the bottom electrode by the alkyl chain and in energy below both Fermi levels ($E_{HOMO} = -5.0$ eV). The HOMO is coupled to the top electrode: at positive bias (here defined as reverse bias) the HOMO does not fall in the energy window defined by both Fermi-levels but at sufficient negative bias (here defined as forward bias) its energy lies within the energy window of both Fermi-levels (Figure 1). Hence, only at forward bias the

Table 1. Properties of the Self-Assembled Monolayers

	CV[a]			UPS[b]					NEXAFS	ARXPS[c]
SAM	Γ ($\times 10^{-10}$ mol/cm^2)	E_{HOMO} (eV)	ΔE_{pa} (eV)	E_{HOMO} (eV)	δE_{ME}	fwhm (eV)	ΔE_{UPS} (eV)	WF (eV)	LUMO (eV)	d (nm)
Fc—Fc	3.96 ± 0.12	−4.93 ± 0.01	0.31 ± 0.01	−5.06	0.82	0.82	0.36	4.24	−2.16	2.23
Fc=Fc$^\beta$	3.49 ± 0.09	−4.76 ± 0.01	0.56 ± 0.01	−4.82	0.56	0.92	0.43	4.26	−2.11	1.92
Fc=Fc$^\alpha$	3.92 ± 0.20	−4.76 ± 0.02	0.63 ± 0.02	−4.74	0.48	0.98	0.52	4.26	−2.13	1.97

[a]The error bar represent the standard deviation from three independent measurements (see Supporting Information page S7 for details). [b]The error is 0.05 eV, which is the resolution of the UPS (see Supporting Information pages S12−S13 for details). [c]The error is 0.20 nm estimated from the error of the fits (see Supporting Information pages S14−S16 for details).
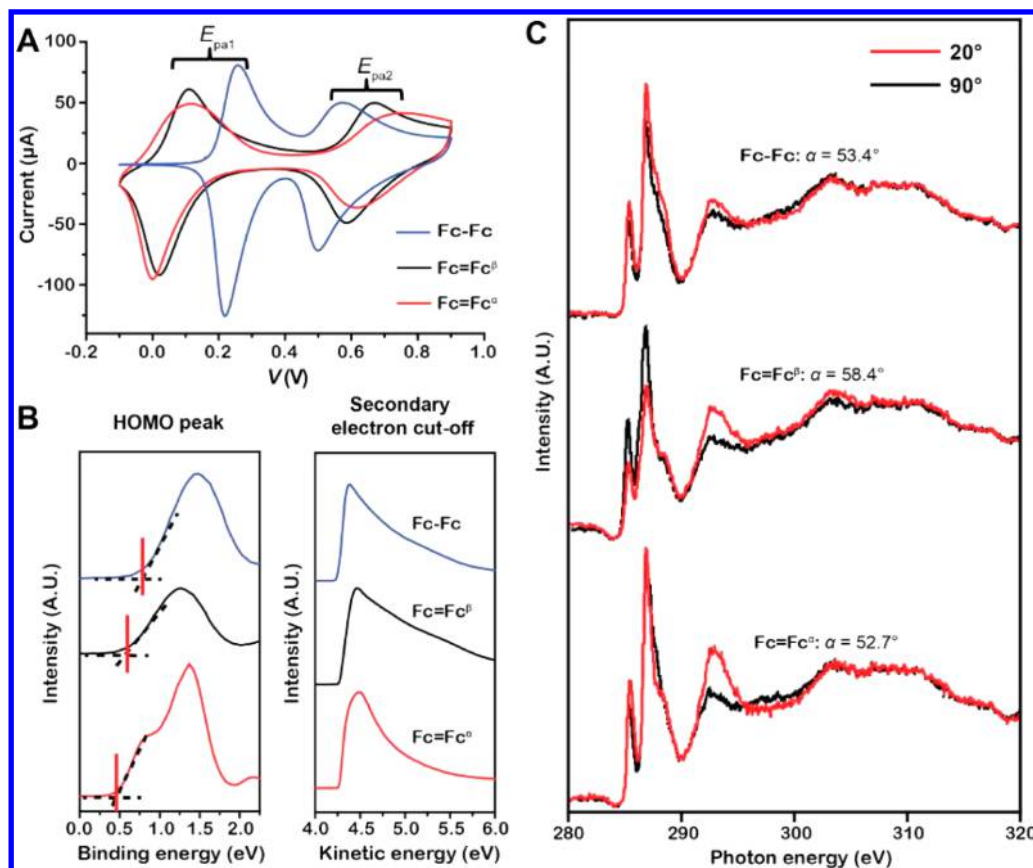

Figure 2. (A) The cyclic voltammograms of the three Au^{TS}-SC$_{11}$Fc$_2$ SAMs as the working electrode, Pt as the counter electrode, and saturated Ag/AgCl as the reference electrode, recorded at a scan rate of 1.0 V/s with aqueous 1.0 M HClO$_4$ as the electrolyte. (B) Valence band and secondary cutoff spectra of the HOMO peak (see Figure S8 for the complete spectra). (C) Angular dependent C K-edge NEXAFS spectra of the SAMs of Ag^{TS}-SC$_{11}$Fc$_2$.

HOMO participates in the mechanism of charge transport resulting in rectification. We do not believe that the LUMO participates in the mechanism of rectification in the applied bias due to the large HOMO−LUMO gap of the Fc$_2$ moieties (see below) as indicated in the energy level diagram. If the LUMO would be energetically accessible at large positive bias this would result in a reduction of R.

We characterized the SAMs with the Fc$_2$ terminal groups (see Figure 1) that were synthesized by previously reported methods[40,41] as follows: cyclic voltammetry (CV) to determine the surface coverage of the Fc$_2$ units Γ_{Fc} (mol/cm^2), angle resolved X-ray photoelectron spectroscopy (XPS) to determine the SAM thickness d (nm), near edge X-ray absorption fine structure spectroscopy (NEXAFS) to determine the tilt angle of the Fc$_2$ units with respect to the surface normal α (deg) and the energy of the LUMO, and ultraviolet photoelectron spectroscopy (UPS) to determine the offset between the Fermi-level of

the bottom-electrode with the HOMO δE_{ME} (eV). Table 1 and Figure 2 summarize the results (see Supporting Information for more details and Figure S6−S8 for all data).

The CVs show that the two Fc moieties are electrochemically strongly coupled and, as expected, the difference in the anodic peak potentials $\Delta E_{pa} = E_{pa,1} - E_{pa,2}$ (with $E_{pa,1}$ and $E_{pa,2}$ being the first and second anodic peak potential, respectively, as indicated in Figure 2A) increases from 0.34 eV for the Fc—Fc SAMs to 0.56 or 0.63 eV for the Fc=Fc$^\beta$ and Fc=Fc$^\alpha$ SAMs. The surface coverage of Fc=Fc$^\beta$ (Table 1) is slightly lower than that for Fc—Fc and Fc=Fc$^\alpha$ because of unfavorable steric repulsions between the head groups. The angle-resolved NEXAFS data reveal that indeed the Fc=Fc$^\beta$ units are more flat-lying than the Fc—Fc and Fc=Fc$^\alpha$ units (Table 1) in accordance with the reduced thickness of the SAMs observed by ARXPS. These flat-lying Fc$_2$ moieties reduce the packing
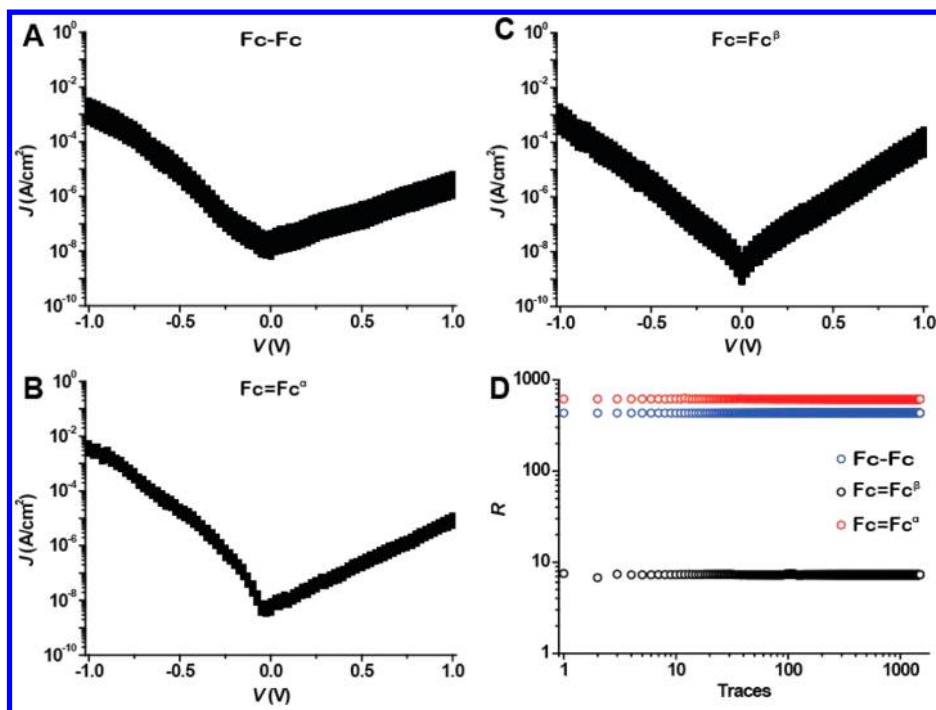
Figure 3. Electrical stability of the junctions: 1500 $J(V)$ curves (trace and retrace) of junctions with SAMs of Fc—Fc (A), Fc=Fc$^\alpha$ (B) and Fc=Fc$^\beta$ (C). D) Plot of R (= J(at −1.0 V)/J(at +1.0 V)) as a function of the trace number.

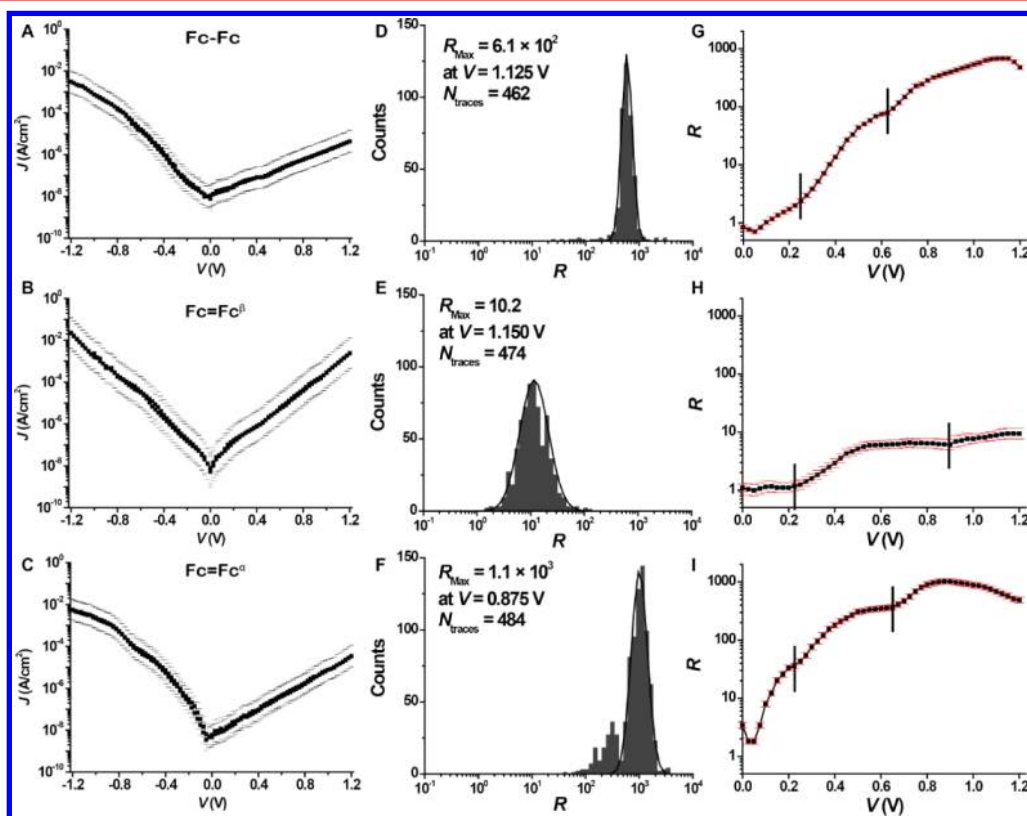**Figure 4.** Log-average $J(V)$ plot of the junctions with SAMs of Fc—Fc (A), Fc=Fc$^\beta$ (B), and Fc=Fc$^\alpha$ (C), the corresponding histograms of R_{max} with a Gaussian fit to these histograms (D−F), and value of R versus applied bias (G−I). The error bars in A−C indicate the log-standard deviations (σ_{log}) and in H−I the 95% confidence levels.

between neighboring molecules in the SAMs and consequently increase the leakage current across the diode (see below).

The energy level diagrams shown in Figure 1 were constructed using the work functions (WF) and the HOMO onset values (δE_{ME}) derived from the UPS data, and the LUMO levels estimated by NEXAFS. Table 1 shows that the work functions are similar (~4.25 ± 0.05 eV), but the values of E_{HOMO} for Fc=Fc$^\beta$ and Fc=Fc$^\alpha$ SAMs are 0.24 to 0.32 eV

lower than that of Fc—Fc in good agreement with the CV data. The full width at half-maximum (fwhm) of the HOMO signal in the UPS spectra increases with increasing electrochemical communication between the Fc units (ΔE_{pa}) and even a shoulder appears in the UPS spectrum of Fc=Fc$^{\alpha}$. This observation implies that an increase of the electrochemical communication between two Fc moieties lowers the E_{HOMO} and consequently reduces δE_{ME} (Table 1). Hence, the signal in the UPS is assigned to the HOMO and HOMO−1, from which we estimated the energy difference between both levels (ΔE_{UPS}; see Table 1 and Figure S9) in good accord with the ΔE_{pa} values. The NEXAFS data suggest that the HOMO−LUMO gap is 2.6−2.9 eV (in agreement with experimental values and the density functional theory (DFT) calculations reported by others)[42] and that the LUMO is ~2 eV above the Fermi levels of the electrodes (Table 1). In contrast, the HOMO levels are 0.5 to 0.8 eV below the Fermi levels of the electrodes according to the UPS data. On the basis of the values in the energy level diagram in Figure 1, we conclude that the HOMO participates in the mechanism of rectification while the LUMO is not energetically accessible in the applied bias window of ±1.2 V. Because NEXAFS tends to underestimate the energy of the empty levels due to core-hole electron interactions, the LUMO levels obtained by NEXAFS can be seen as a lower limit value (see page S19).[43]

The SAM-based junctions with cone-shaped tips of GaO$_x^{cond}$/EGaIn were fabricated following previously reported procedures.[29] We grounded the bottom-electrode using a gold probe penetrating the SAMs and the top-electrode of GaO$_x^{cond}$/EGaIn was biased from 0 V → 1.0 V → 0 V → −1.0 V → 0 V with a step size of 50 mV. In this bias range, the junctions are stable and the yield in nonshorting junctions is ~90% (as shown in Supporting Information). To study R as a function of bias, we reduced the step size to 25 mV and increased the bias range to ±1.2 V; this increase of the bias range decreased the yield of nonshorting junctions to ~71%. We recorded and analyzed statistically large numbers of J(V) curves (450−524 traces) following previously reported procedures. To the histograms of log$_{10}$|J| (and log$_{10}$|R|) we fitted Gaussians to determine the log-mean values of J (or R) and their log standard-deviations (σ_{log}). The Z-test was used to calculate the 95% confidence intervals (see page S5 in the Supporting Information).

To characterize the stability of the diodes, we used EGaIn top-electrodes stabilized in a through-hole PDMS (polydimethylsiloxane; the fabrication is detailed in ref 44) and cycled the applied voltage for 1500 times (one cycle = 0 V → 1.0 V → 0 V → −1.0 V → 0 V). The details of the fabrication of the top-electrodes and junctions can be found in ref 44 and the Supporting Information. Figure 3A−C show the 1500 J(V) traces (cycles) of all three SAMs. According to the data in Figure 3D, R (at ±1.0 V) remained unchanged during this experiment apart from a small decrease in current (see Supporting Information, Figure S11). This observation of stable rectification from the SAMs with the biferrocenylene terminal groups is in good agreement with the redox stability of these SAMs monitored by CV measurements.[41] The fact that the values of R do not change as a function of the cycle number despite the large applied bias indicates that the Ga$_2$O$_3^{cond}$ layer does not change, i.e., anodic growth of the Ga$_2$O$_3^{cond}$ layer does not occur.[45]

Figure 4 shows the log-average J(V) traces, the values of R versus V, and histograms of R for applied V at the highest value of R (R_{max}) of the three types of junctions. The most striking

observation is that the junctions with Fc=Fc$^{\beta}$ SAMs perform poorly with an R_{max} = 10.2 (σ_{log} = 2.6) at ±1.150 V while the other diodes have higher values of R_{max} of 6.1×10^2 (σ_{log} = 2.3) at ±1.125 V for junctions with Fc—Fc and 1.1×10^3 (σ_{log} = 2.4) at ±0.875 V for junctions with Fc=Fc$^{\alpha}$, respectively. This large difference in R_{max} is caused by the large leakage current (that is, the current at positive bias) for junctions with SAMs of Fc=Fc$^{\beta}$. (The values of J when the diodes are in the on-state, that is, at −1.2 V, are similar for all the junctions.)

To investigate the mechanism of rectification in more detail, we determined the bias dependency of the value of R over the bias range of ±1.2 V (Figure 4G−I). We make two important observations. The turn-on voltage (defined as the voltage at which the value of R increases sharply as indicated by the vertical bars in Figure 4G−I) is smaller for junctions with Fc=Fc$^{\alpha}$ (0.225 V) and Fc=Fc$^{\beta}$ (0.225 V) and slightly larger for Fc—Fc (0.250 V) junctions. Beyond 0.6 V, another sharp increase of R is visible for all three SAMs as indicated by the second vertical bar, for Fc—Fc at 0.625 V, Fc=Fc$^{\alpha}$ at 0.650 V and Fc=Fc$^{\beta}$ at 0.900 V.

We explain these observations as follows. The turn-on values are directly related to the δE_{ME} values and decrease with decreasing δE_{ME}. In other words, the HOMO level is close in energy to the Fermi levels and can fall within the energy window defined by the two Fermi-levels of the electrodes at relatively low applied bias. Although the exact values of δE_{ME} inside the junctions will likely be smaller than the ones measured by UPS,[46] it seems that the values measured by UPS correlate well with the turn-on voltages of the junctions. Now the HOMO−1 comes into resonance providing a second tunneling channel, that is, through the HOMO and HOMO−1 orbitals. Consequently, these diodes with two conduction channels have a factor of ~10 higher currents in the on-state than diodes based on SC$_{11}$Fc with only one conduction channel[28,30,35] (the leakage currents of these two systems are similar) causing the 10-fold improvement in the value of R.

So far we have ignored the role of the LUMO levels in the mechanism of rectification because of the large HOMO−LUMO gap as explained above.[30,47] One could argue that due to renormalization[48−50] of the energy levels (induced by charges on the molecule and the corresponding image charges in the electrodes during charge transport) the LUMO levels may be important during charge transport. The difference in energy between the HOMO and HOMO−1 orbitals can be estimated from the R(V) plot and is roughly 0.4 eV for junctions with Fc=Fc$^{\alpha}$ (where the two steps are clearly visible in the R(V) plot). This value is about 1.5 times smaller than the value estimated by CV or UPS which could be the result of renormalization. In this case, the HOMO−LUMO gap would also be smaller by a factor of 1.5. Thus, during charge transport the LUMO would be lowered (estimated by NEXAFS) to 1.3 eV above the Fermi-levels. The decrease in the value of R at large applied bias (which is clearly visible in Figure 4I) might be an indication that the LUMO participates in the mechanism of charge transport. Other factors, however, such as broadening of the HOMO level once contacted with top-electrode[35] or a finite potential drop at the SAM//top electrode interface,[30] could also cause a reduction of the value of R at large applied bias.

To explain the poor performance of the junctions with SAMs of Fc=Fc$^{\beta}$, we have to take the supramolecular structure of the junction into consideration. On the basis of the UPS and CV results, the electronic properties of both Fc=Fc$^{\beta}$ and Fc=Fc$^{\alpha}$

junctions are similar but yet their performance vastly differs. From a supramolecular point of view, the Fc=Fc$^\beta$ moiety with the alkyl chain connected to the 3-position displays a low value of α which, consequently, results in large steric repulsions between neighboring Fc=Fc units and thus lower SAM packing energies. Such loosely packed SAMs are prone to defects during the fabrication of the junctions resulting in large leakage currents and consequently low values of R. In contrast, an alkyl chain in the 2-position of Fc=Fc results in molecular diodes with very good properties. Thus, an apparently small change in the chemical structure can have a dramatic effect on the supramolecular structure of the SAM, while leaving the electronic structure almost unchanged, which in turn result in a dramatic change in the performance of the molecular diodes in terms of rectification ratios.

In summary, we found that EGaIn junctions with SAMs of Fc=Fc$^\alpha$ rectify currents with large values of $R \sim 1.1 \times 10^3$ at 0.875 V. This large value of R was achieved by a combination of three factors: (i) optimization of the electronic structure to minimize the turn-on voltage, (ii) optimization of the supramolecular structure to minimize the leakage currents of the junctions, and (iii) involvement of two molecular orbitals (HOMO and HOMO−1) in the mechanism of rectification to increase the currents in the on-state. Although these improvements demonstrate that molecular diodes can have large rectification ratios, the values reported here are still lower than those of commercially available Si-based diodes. However, the results shown here indicate that molecular diodes with large values of R are possible and that perhaps further improvements may result in molecular diodes with even larger values of R.

■ ASSOCIATED CONTENT

Ⓢ Supporting Information

The Supporting Information is available free of charge on the ACS Publications website at DOI: 10.1021/acs.nano-lett.5b02014.

> Details of the synthesis of the molecules, fabrication of the bottom-electrodes, fabrication of the junctions, statistical analysis, electrochemical characterization of the SAMs, and photoelectron spectroscopy and near-edge X-ray absorption fine structure spectroscopy. (PDF)

■ AUTHOR INFORMATION

Corresponding Author

*E-mail: christian.nijhuis@nus.edu.sg.

Notes

The authors declare no competing financial interest.

■ ACKNOWLEDGMENTS

■ REFERENCES

(1) Manrique, D. Z.; Huang, C.; Baghernejad, M.; Zhao, X.; Al-Owaedi, O. A.; Sadeghi, H.; Kaliginedi, V.; Hong, W.; Gulcur, M.; Wandlowski, T.; Bryce, M. R.; Lambert, C. J. *Nat. Commun.* **2015**, *6*, 6389.

(2) Fracasso, D.; Valkenier, H.; Hummelen, J. C.; Solomon, G. C.; Chiechi, R. C. *J. Am. Chem. Soc.* **2011**, *133* (24), 9556−9563.

(3) Tan, S. F.; Wu, L.; Yang, J. K. W.; Bai, P.; Bosman, M.; Nijhuis, C. A. *Science* **2014**, *343* (6178), 1496−1499.

(4) Schuller, J. A.; Barnard, E. S.; Cai, W. S.; Jun, Y. C.; White, J. S.; Brongersma, M. L. *Nat. Mater.* **2010**, *9* (3), 193−204.

(5) Mahato, R. N.; Lulf, H.; Siekman, M. H.; Kersten, S. P.; Bobbert, P. A.; de Jong, M. P.; De Cola, L.; van der Wiel, W. G. *Science* **2013**, *341* (6143), 257−260.

(6) Fan, F. R. F.; Yang, J. P.; Cai, L. T.; Price, D. W.; Dirk, S. M.; Kosynkin, D. V.; Yao, Y. X.; Rawlett, A. M.; Tour, J. M.; Bard, A. J. *J. Am. Chem. Soc.* **2002**, *124* (19), 5550−5560.

(7) Cui, X. D.; Zarate, X.; Tomfohr, J.; Sankey, O. F.; Primak, A.; Moore, A. L.; Moore, T. A.; Gust, D.; Harris, G.; Lindsay, S. M. *Nanotechnology* **2002**, *13* (1), 5−14.

(8) Dimitrakopoulos, C. D.; Malenfant, P. R. L. *Adv. Mater.* **2002**, *14* (2), 99−100.

(9) Venkataraman, L.; Klare, J. E.; Nuckolls, C.; Hybertsen, M. S.; Steigerwald, M. L. *Nature* **2006**, *442* (7105), 904−907.

(10) Akkerman, H. B.; de Boer, B. *J. Phys.: Condens. Matter* **2008**, *20* (1), 013001.

(11) Mujica, V.; Ratner, M. A.; Nitzan, A. *Chem. Phys.* **2002**, *281* (2−3), 147−150.

(12) Aradhya, S. V.; Venkataraman, L. *Nat. Nanotechnol.* **2013**, *8* (6), 399−410.

(13) Vincent, R.; Klyatskaya, S.; Ruben, M.; Wernsdorfer, W.; Balestro, F. *Nature* **2012**, *488* (7411), 357−360.

(14) Kornilovitch, P. E.; Bratkovsky, A. M.; Williams, R. S. *Phys. Rev. B: Condens. Matter Mater. Phys.* **2002**, *66* (16), 165436.

(15) Liu, R.; Ke, S. H.; Yang, W. T.; Baranger, H. U. *J. Chem. Phys.* **2006**, *124* (2), 024718.

(16) Batra, A.; Darancet, P.; Chen, Q.; Meisner, J. S.; Widawsky, J. R.; Neaton, J. B.; Nuckolls, C.; Venkataraman, L. *Nano Lett.* **2013**, *13* (12), 6233−6237.

(17) Mativetsky, J. M.; Pace, G.; Elbing, M.; Rampi, M. A.; Mayor, M.; Samori, P. *J. Am. Chem. Soc.* **2008**, *130* (29), 9192−9193.

(18) Aviram, A.; Ratner, M. A. *Chem. Phys. Lett.* **1974**, *29* (2), 277−283.

(19) Lenfant, S.; Krzeminski, C.; Delerue, C.; Allan, G.; Vuillaume, D. *Nano Lett.* **2003**, *3* (6), 741−746.

(20) Diez-Perez, I.; Hihath, J.; Lee, Y.; Yu, L. P.; Adamska, L.; Kozhushner, M. A.; Oleynik, II; Tao, N. J. *Nat. Chem.* **2009**, *1* (8), 635−641.

(21) Elbing, M.; Ochs, R.; Koentopp, M.; Fischer, M.; von Hanisch, C.; Weigend, F.; Evers, F.; Weber, H. B.; Mayor, M. *Proc. Natl. Acad. Sci. U. S. A.* **2005**, *102* (25), 8815−8820.

(22) Yee, S. K.; Sun, J. B.; Darancet, P.; Tilley, T. D.; Majumdar, A.; Neaton, J. B.; Segalman, R. A. *ACS Nano* **2011**, *5* (11), 9256−9263.

(23) Stadler, R.; Geskin, V.; Cornil, J. *J. Phys.: Condens. Matter* **2008**, *20* (37), 374105.

(24) Shumate, W. J.; Mattern, D. L.; Jaiswal, A.; Dixon, D. A.; White, T. R.; Burgess, J.; Honciuc, A.; Metzger, R. M. *J. Phys. Chem. B* **2006**, *110* (23), 11146−11159.

(25) Ashwell, G. J.; Tyrrell, W. D.; Whittam, A. J. *J. Am. Chem. Soc.* **2004**, *126* (22), 7102−7110.

(26) Capozzi, B.; Xia, J.; Adak, O.; Dell, E. J.; Liu, Z.-F.; Taylor, J. C.; Neaton, J. B.; Campos, L. M.; Venkataraman, L. *Nat. Nanotechnol.* **2015**, *10* (6), 522−527.

(27) Ashwell, G. J.; Urasinska, B.; Tyrrell, W. D. *Phys. Chem. Chem. Phys.* **2006**, *8* (28), 3314−3319.

(28) Yuan, L.; Jiang, L.; Thompson, D.; Nijhuis, C. A. *J. Am. Chem. Soc.* **2014**, *136* (18), 6554−6557.

(29) Nerngchamnong, N.; Yuan, L.; Qi, D. C.; Li, J.; Thompson, D.; Nijhuis, C. A. *Nat. Nanotechnol.* **2013**, *8* (2), 113−118.

(30) Nijhuis, C. A.; Reus, W. F.; Siegel, A. C.; Whitesides, G. M. *J. Am. Chem. Soc.* **2011**, *133* (39), 15397−15411.

(31) Nijhuis, C. A.; Reus, W. F.; Whitesides, G. M. *J. Am. Chem. Soc.* **2009**, *131* (49), 17814−17827.

(32) Jiang, L.; Yuan, L.; Cao, L.; Nijhuis, C. A. *J. Am. Chem. Soc.* **2014**, *136* (5), 1982−1991.

(33) Honciuc, A.; Jaiswal, A.; Gong, A.; Ashworth, H.; Spangler, C. W.; Peterson, I. R.; Dalton, L. R.; Metzger, R. M. *J. Phys. Chem. B* **2005**, *109* (2), 857−871.

(34) Van Dyck, C.; Ratner, M. A. *Nano Lett.* **2015**, *15* (3), 1577−1584.

(35) Yuan, L.; Nerngchamnong, N.; Cao, L.; Hamoudi, H.; del Barco, E.; Roemer, M.; Sriramula, R. K.; Thompson, D.; Nijhuis, C. A. *Nat. Commun.* **2015**, *6*, 6324.

(36) Nijhuis, C. A.; Reus, W. F.; Barber, J. R.; Dickey, M. D.; Whitesides, G. M. *Nano Lett.* **2010**, *10* (9), 3611−3619.

(37) Jeong, H.; Kim, D.; Wang, G.; Park, S.; Lee, H.; Cho, K.; Hwang, W.-T.; Yoon, M.-H.; Jang, Y. H.; Song, H.; Xiang, D.; Lee, T. *Adv. Funct. Mater.* **2014**, *24* (17), 2472−2480.

(38) Müller-Meskamp, L.; Karthäuser, S.; Zandvliet, H. J. W.; Homberger, M.; Simon, U.; Waser, R. *Small* **2009**, *5* (4), 496−502.

(39) Mentovich, E. D.; Rosenberg-Shraga, N.; Kalifa, I.; Gozin, M.; Mujica, V.; Hansen, T.; Richter, S. *J. Phys. Chem. C* **2013**, *117* (16), 8468−8474.

(40) Dong, T.-Y.; Chang, L.-S.; Tseng, I. M.; Huang, S.-J. *Langmuir* **2004**, *20* (11), 4471−4479.

(41) Breuer, R.; Schmittel, M. *Organometallics* **2012**, *31* (18), 6642−6651.

(42) Warratz, R.; Aboulfadl, H.; Bally, T.; Tuczek, F. *Chem. - Eur. J.* **2009**, *15* (7), 1604−1617.

(43) Stohr, J. *NEXAFS Spectroscopy*; Springer: Berlin, 1992.

(44) Wan, A.; Jiang, L.; Sangeeth, C. S. S.; Nijhuis, C. A. *Adv. Funct. Mater.* **2014**, *24* (28), 4442−4456.

(45) Wimbush, K. S.; Fratila, R. M.; Wang, D.; Qi, D.; Liang, C.; Yuan, L.; Yakovlev, N.; Loh, K. P.; Reinhoudt, D. N.; Velders, A. H.; Nijhuis, C. A. *Nanoscale* **2014**, *6* (19), 11246−11258.

(46) Levine, I.; Weber, S. M.; Feldman, Y.; Bendikov, T.; Cohen, H.; Cahen, D.; Vilan, A. *Langmuir* **2012**, *28* (1), 404−415.

(47) Kitagawa, K.; Morita, T.; Kimura, S. *J. Phys. Chem. B* **2005**, *109* (29), 13906−13911.

(48) Kaasbjerg, K.; Flensberg, K. *Nano Lett.* **2008**, *8* (11), 3809−3814.

(49) Barr, J. D.; Stafford, C. A.; Bergfield, J. P. *Phys. Rev. B: Condens. Matter Mater. Phys.* **2012**, *86* (11), 115403.

(50) Heimel, G.; et al. *Nat. Chem.* **2013**, *5* (3), 187−194.

(51) Cademartiri, L.; Thuo, M. M.; Nijhuis, C. A.; Reus, W. F.; Tricard, S.; Barber, J. R.; Sodhi, R. N. S.; Brodersen, P.; Kim, C.; Chiechi, R. C.; Whitesides, G. M. *J. Phys. Chem. C* **2012**, *116* (20), 10848−10860.

(52) Sangeeth, C. S. S.; Wan, A.; Nijhuis, C. A. *J. Am. Chem. Soc.* **2014**, *136* (31), 11134−11144.

(53) Simeone, F. C.; Yoon, H. J.; Thuo, M. M.; Barber, J. R.; Smith, B.; Whitesides, G. M. *J. Am. Chem. Soc.* **2013**, *135* (48), 18131−18144.

(54) Nijhuis, C. A.; Reus, W. F.; Whitesides, G. M. *J. Am. Chem. Soc.* **2010**, *132* (51), 18386−18401.